Impedance Optimization of Sirius Stripline Kicker

CNPEM

TUPB006

Henrique de Oliveira Caiafa Duarte and *Sergio Rodrigo Marques*

Brazilian Synchrotron Light Laboratory, Campinas, São Paulo, Brazil.

LNLS sirius

Abstract

Two approaches to design a transverse feedback (TFB) stripline kicker are well known in the accelerators community: one with bare strips in a tapered cavity and other whose shrouded strips are ended with parallel-plate capacitive gaps. This work presents a comparison between both models in terms of electromagnetic performance, proposes alternative solutions for increasing the gap capacitance and analyzes the performance of a hybrid stripline kicker design.

1. Geometry Alternatives

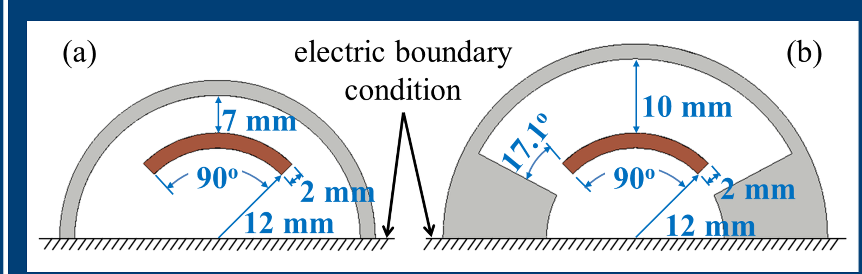

Figure 1: Considered transverse profiles: a) Bare Strip ($g_\perp$=1.09) and b) Shrouded Strip ($g_\perp$=1.01) designs.

$$\kappa^{SB}_{loss,geom} = \frac{1}{\pi}\int_0^\infty Re\,[Z_\parallel(\omega)]\, e^{-\left(\omega\sigma_s/c\right)^2} d\omega \quad (1)$$

$$\kappa^{MB}_{loss,geom} = \frac{M\omega_0}{\pi}\sum_{p=1}^{\infty} Re\,[Z_\parallel(pM\omega_0)]\, e^{-\left(pM\omega_0\sigma_s/c\right)^2} \quad (2)$$

Table 1: Geometric single-bunch (Eq. 1) and multi-bunch (Eq. 2) loss factor comparison among the three designs from Fig. 1, for two bunch length σ_s scenarios.

Geometry Type	Geometric κ_{loss}, mV/pC			
	σ_s = 2.65 mm		σ_s = 3.8 mm	
	SB	MB	SB	MB
Tapered Cavity	614.7	559.7	423.9	361.6
Capacitive Gap	74.9	43.2	48.5	21.8
Hybrid	131.2	75.3	84.9	40.6

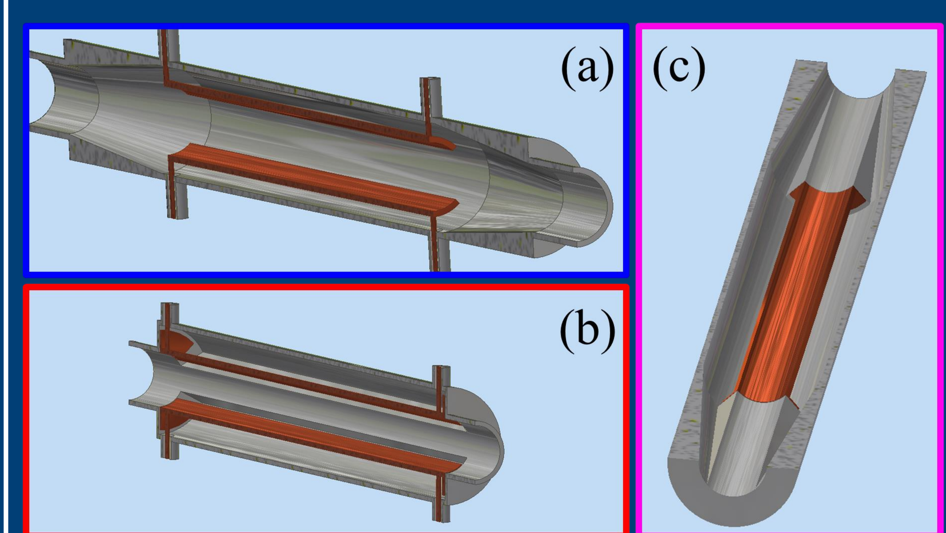

Figure 2: Simulation models of three different stripline concepts. a) The Tapered Cavity Stripline (based on NSLS-II design) consists of Bare Strips (see Fig. 1) placed inside a 1/15 linearly tapered cavity that reaches the 24 mm diameter vacuum chamber profile on both ends. b) The Capacitive Gap one (based on SOLEIL design), consists of Shrouded striplines (see Fig. 1) with 0.5 mm capacitive gaps at both ends and follows the vacuum chamber profile. c) The Hybrid design consists of the Bare Strips ended by capacitive gaps. In the horizontal plane, the round profile gets complete after the 1/15 taper.

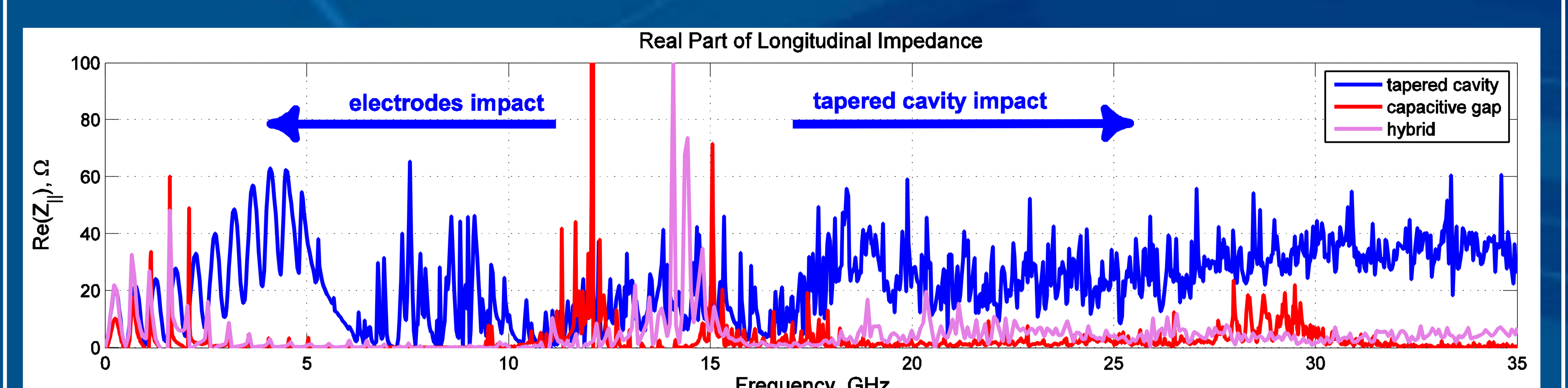

Figure 3: Real part of longitudinal impedance of the Tapered Cavity, Capacitive Gap and Hybrid striplines.

Despite stronger HOMs, Capacitive Gap type was chosen since its feedthroughs receive lower beam load. Alternative gap geometries were further analysed, as shown by Fig. 4

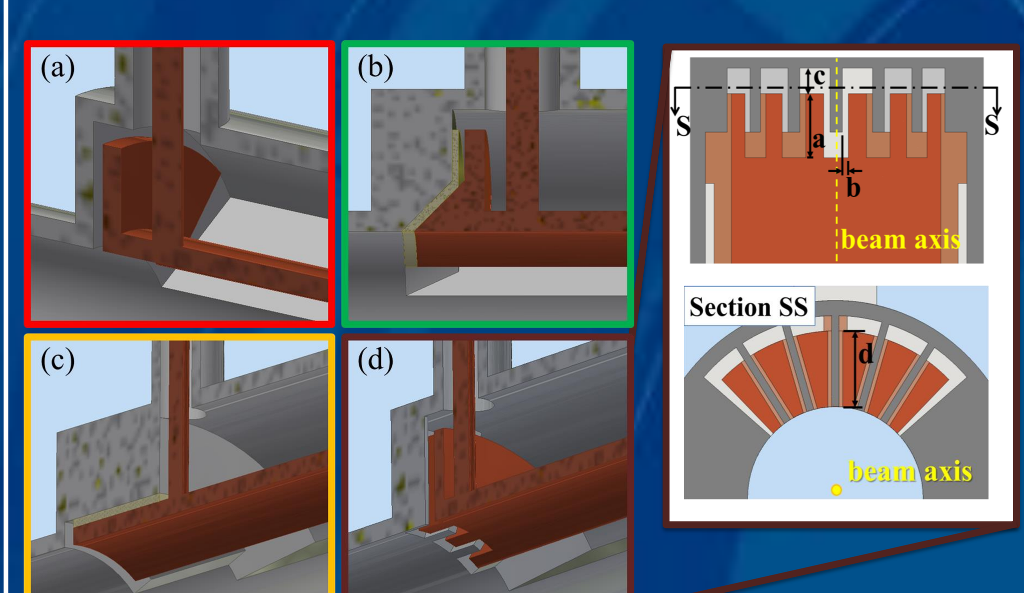

Table 2: Geometric SB and MB loss factor comparison among the four designs from Fig. 4, for two bunch length scenarios.

Gap Type	Geometric κ_{loss}, mV/pC			
	σ_s = 2.65 mm		σ_s = 3.8 mm	
	SB	MB	SB	MB
Standard	74.9	43.2	48.5	21.8
Sliding	45.2	17.4	30.8	8.2
Upper	202	185.5	94.7	79.5
Comb-type	35.5	40	24.6	23.7

Figure 4: Considered alternative gap types for increasing the gap capacitance and allowing alternative mechanical solutions for expected thermal expansions. a) Standard Gap: previous Capacitive Gap. b) Sliding Gap: 1 mm longitudinal gap, 0.5 mm thick alumina ceramics. c) Upper Gap: 20 mm long and 1 mm thick alumina ceramics. d) Comb-type Gap: *a* = 5 mm, *b* = 0.5 mm, *c* = 2mm and *d* = 10 mm.

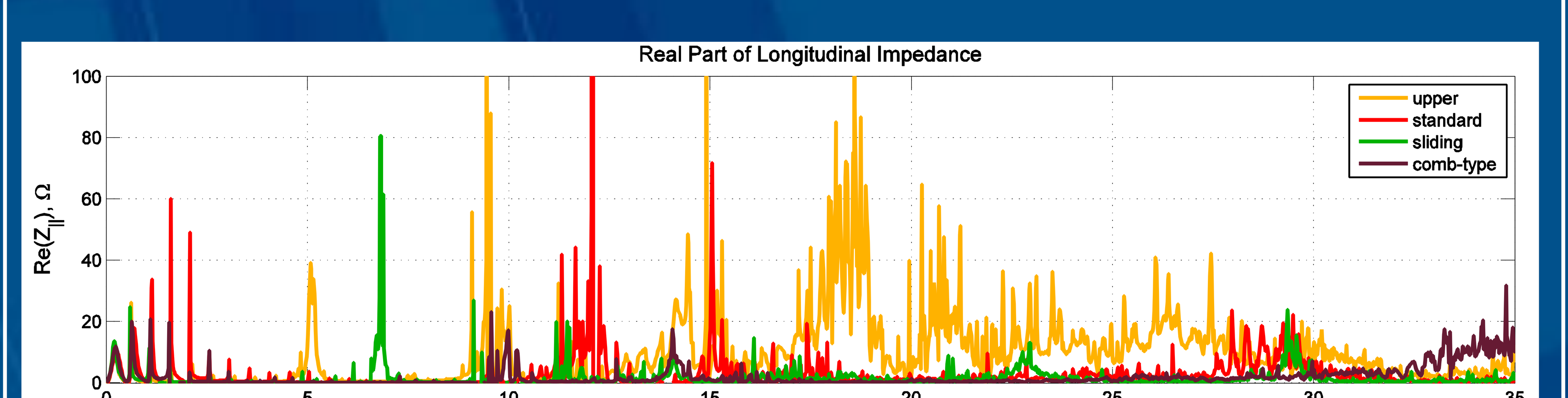

Figure 5: Comparison between the real part of longitudinal beam impedance of the Standard, Sliding, Upper and Comb-type Capacitive Gap striplines.

Comb-type Gap was chosen due to low loss factor, weak HOMs and since no ceramics brazing is needed.

2. S1,1 Optimization

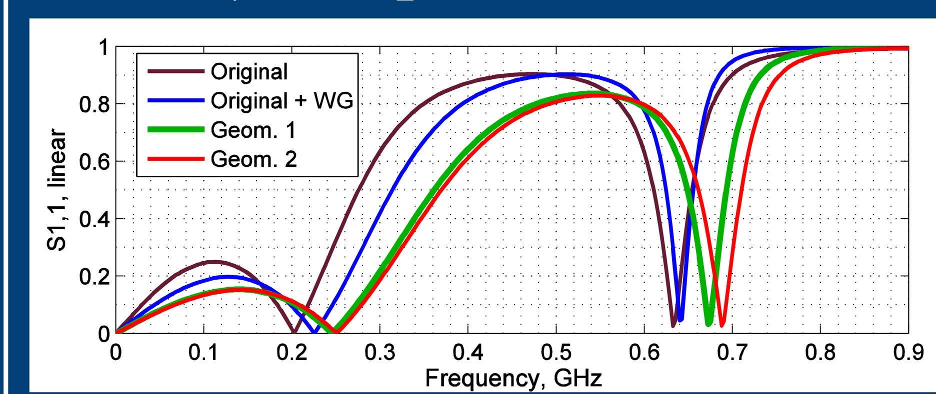

Figure 6: S1,1 parameters evolution stages. In the first (blue curve), a rectangular waveguide (WG), centered with the pin, was inserted between the coaxial line and the gap teeth in order to add an inductive component, but was not enough for achieving the desired goal. In the second stage (green & red curves), as shown by Fig. 7, two alternative geometries for reducing the gap capacitance have been designed. Both reached -16.4 dB (15%) maximum within the 250 MHz BW.

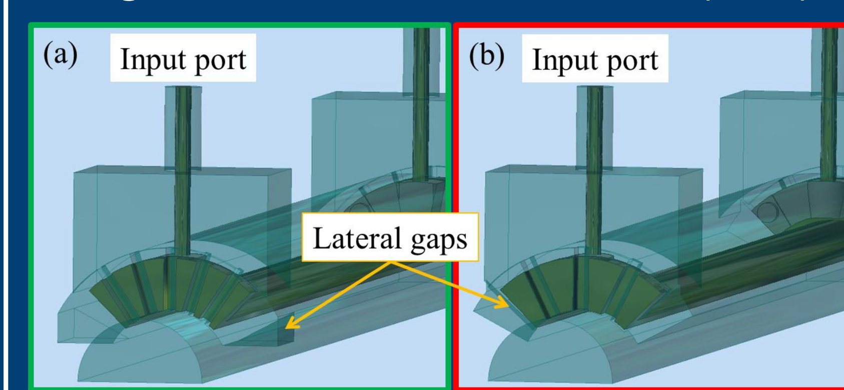

Figure 7: a) Geom. 1 has the gap between teeth *b* = 0.7 mm and the lateral gaps increased. b) Geom. 2 has 4 teeth instead of 6 and kept the comb-type geometry parameters *a*–*d* to their original values.

Geom. 2 was preferred: 55.15 mV/pC and 42.91 mV/pC SB and MB loss factors, respectively. Geom 2: 29% and 84% higher.

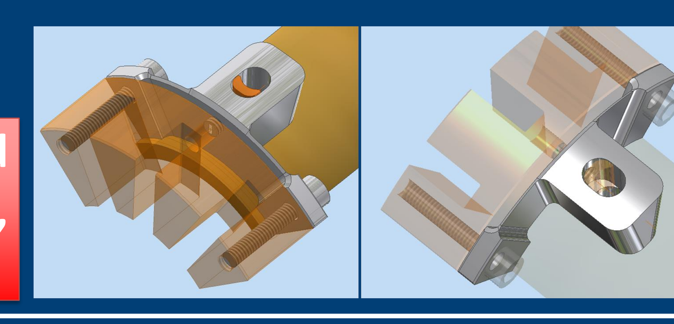

Figure 8: Feedthrough pin holder considered in the simulations.

3. Vertical Shunt Impedance

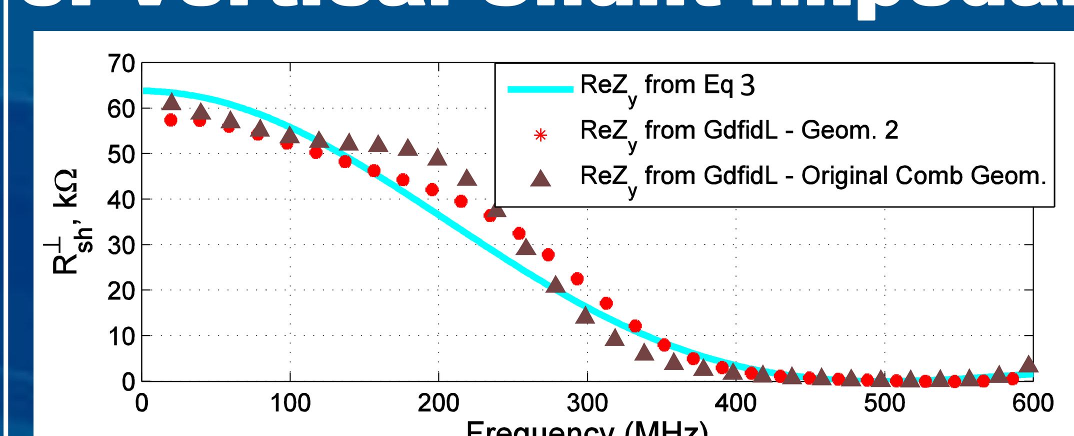

Figure 9: Shunt impedance obtained from Eqs. 3 and 4 (cyan curve) compared with the ones from Eq. 4 and simulated vertical coupling impedances for Geometry 2 (red asterisk) and original Comb-type Gap design (brown triangle). Good agreement was found.

The gap capacitance interferes with the shunt impedance frequency response by distorting the symmetry of the vertical impedance's fundamental mode.

$$Z_\perp(k) = \frac{g_\perp^2 Z_{ch,\perp}}{kr^2}[\sin^2(kL) + j\sin(kL)\cos(kL)] \quad (3) \qquad R^\perp_{sh} = \frac{4\times Re(Z_\perp(k))}{k} \quad (4)$$

4. Thermo-mechanical Analysis

Using GdfidL resistive wall (RW) boundary conditions (for I_{av} = 500 mA and σ_s = 2.65 mm):

$$P_{loss} = \frac{2\pi}{M\omega_0}\left(\kappa^{MB}_{loss,RW} - \kappa^{MB}_{loss,geom}\right) I_{av}^2 = 5.86\ W$$

Still more conservative! x2

Table 3: Dissipated power among the geometry parts.

Component	Material	Power, %	Power, W
Cav. + end pipes	SS	33.17	3.888
Cavity ridges	SS	39.97	4.685
WG + outer coax.	SS	2.91	0.341
Stripline (SL)	Cu	8.57	1.004
SL teeth	Cu	1.48	0.173
Chamber teeth	SS	10.85	1.271
Feedthrough pins	SS	1.04	0.122
Holder slits	SS	0.53	0.062
Holder–center	SS	1.01	0.118
Holder–sides	SS	0.47	0.055

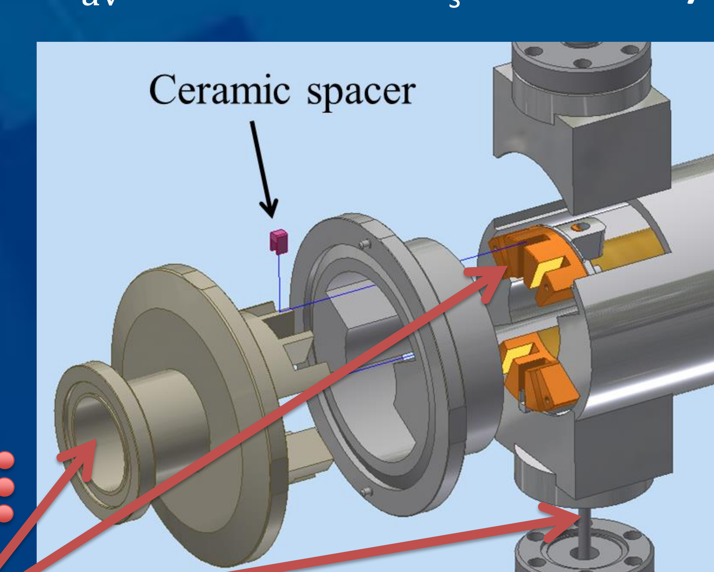

Figure 10: Mechanical design of the stripline kicker. A 5 mm thick alumina washer was considered in the feedthrough. Commercial ones will be used and a kicker prototype is scheduled for late this year.

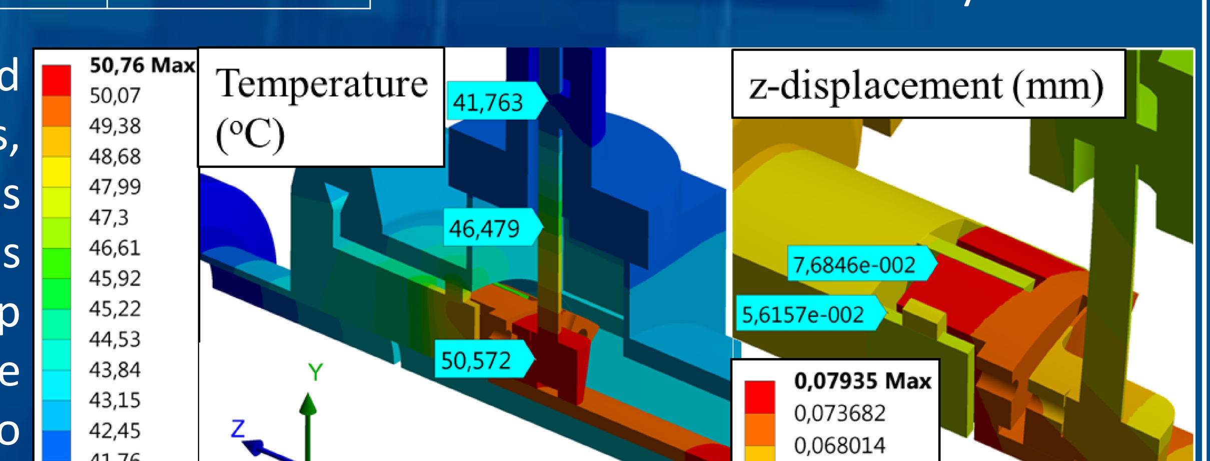

Figure 11: Thermal (left) and mechanical (right) simulations, where 80x distortion magnification is shown. Mechanical results provides only 20 µm longitudinal gap contraction and also shows that the holder was not optimized in order to avoid the pin bending. Even though the found von Misses equivalent stress (80 MPa) is much below ceramics breaking point, the pin holder will be optimized to reduce the stresses at the feedthrough.

Acknowledgement

The authors would like to thank not only T.M. Rocha (from LNLS Vacuum Group) for his tremendous support and execution of the mechanical design and thermal simulations, but also E. Plouviez, G. Rehm, A. Morgan and J.J. Sebek for the fruitful discussions. Last but not least, special thanks must go to SINAPAD colleagues for the clusters infrastructure and their excellent technical support.